Prediction of mechanical properties in bimodal nanotwinned metals with a composite structure

Linli Zhu[1*], Xiang Guo[2], Haihui Ruan[3] and Jian LU[4]

[1]Department of Engineering Mechanics, School of Aeronautics and Astronautics, Zhejiang University, Hangzhou 310027, Zhejiang Province, China

[2]School of Mechanical Engineering, Tianjin University, Tianjin 300072, China

[3]Department of Mechanical Engineering, The Hong Kong Polytechnic University, Hong Kong, China

[4]Department of Mechanical and Biomedical Engineering, City University of Hong Kong, Kowloon, Hong Kong, China

Abstract

Nanostructured face-centered cubic (fcc) metals with nanoscale twin lamellae and multiple distribution of microstructural size are proved to possess higher yield strength and good ductility. In this paper, a mechanism-based theoretical model is developed to simulate the yield strength, strain hardening, and uniform elongation of the nanotwinned composite metals with bimodal distribution of microstructural size. The mechanisms of strengthening and the failure in such bimodal nanotwinned metals are studied for evaluating the strength and ductility. A modified mean-field approach is adopted here to calculate the total stress-strain response of this kind of nanotwinned composite structures. The contribution of microcracks generated during plastic deformation has been taken into account to predict strain hardening and uniform elongation. Our simulation results indicate that the proposed model can successfully describe the mechanical properties of bimodal nanotwinned metals with a composite structure, including the yield strength and ductility. We further demonstrate that the yield strength and elongation are both sensitive to the twin spacing and the volume fraction of components. The calculations based on the proposed model agree well with the experimental results. These findings suggest that the high yield strength and

[*]Author to whom correspondence should be addressed; electronic mail: llzhu@zju.edu.cn (Linli Zhu).

high ductility can be achieved by optimizing the grain size and the twin spacings in the nanotwinned composite structures.

Key Words: Bimodal nanotwinned metal; Twin spacing; Grain Size; Yield strength; Ductility.

1 Introduction

Nanostructured metals have stimulated vast interests due to their distinctive mechanical properties, for example, the superior mechanical strength compared to those of corresponding coarse-grained counterparts [1-7], which make these materials play the essential role in designing lighter and stronger structures of technological applications. Unfortunately, the improved strength in nanostructured metals is always achieved with the loss of ductility and work-hardening capability [3,4,8-13], which is similar to the traditional strengthening methods such as refining grain size, solid solution alloying and phase transformation. Therefore, how to achieve the simultaneously higher strength and ductility in metals and alloys is the essentially challenging issue in the application of the nanostructured metals. In the past ten years a great number of endeavors have been made to explore how to improve the strength with keeping good ductility and toughness. Mixing the various sizes of microstructures in nanostructured metals have been proved as an effective approach for a superior synergy in strength and ductility. For example, the nanostructured metallic materials with bi/multi-modal grain size distribution perform higher yield strength with a good ductility [14-23]. Generating the intrinsic twin boundaries in polycrystalline metals is also an alternative method to improve the tensile ductility in higher-strength nanostructured metals, such as the nanotwinned polycrystalline coppers and nanotwinned stainless steels [24-28]. More recently, a novel strategy is developed to strengthen the metallic materials by means of dynamic plastic deformation to embed the nanotwinned grains into the matrix of nano-sized grains or coarse-grains. Such nanotwinned composites with bimodal distribution of microstructural size exhibit the excellent combination of strength and ductility [29-32].

After discovering the effective methodologies in experiments for enhancing the strength-ductility synergy, a plenty of theoretical studies have been carried out to investigate the deformation mechanisms and then to predict the corresponding mechanical properties. In general, micromechanical models and finite element methods are widely utilized to simulate the stress-strain response in the composite nanomaterials such as the particle reinforced metals matrix composites and nanograins/nanotwins strengthened composite metallic materials [20-23,33-38]. For the nanotructured metals with a bimodal grain size distribution, the secant Mori-Tanaka (M-T) mean-field approach [20,21,39] and the viscoplastic self-consistent scheme [40,41] are often applied to simulate the yield strength and ductility of such composite structure, which are sensitive to the grain size distribution and volume fraction of component. For the nanotwinned polycrystalline metals, the molecular dynamic (MD) simulations are performed usually in the atomic scale to quantify the contributions of the twin boundaries (TBs) to the strength, strain hardening and toughness [42-47]. The mechanism-based theoretical models with a continuum description are presented to describe the mechanical behaviors in the nanotwinned metal. For example, the crystal plasticity models for nanotwinned copper were developed to simulate the stress-strain response as well as the fracture behaviors by finite element method [38, 48-50]. The dislocation density-based plasticity models were developed to describe the variation of strength, strain hardening and the ductility of nanotwinned metals with the twin spacing, and a scale law of the maximum strength in nanotwinned metals was explored [51-54]. However, for the nanotwinned composite metals, it remains unclear how to predict the mechanical properties as the functions of grain size, twin spacing, and volume fraction of each component. The explicit theoretical model that enables to describe the experimental results is still in lack.

In this work, a micromechanical composite model is developed to study the mechanical properties of nanotwinned composites with a bimodal distribution of microstructural size. The mechanism-based plastic model for nanotwinned metals is adopted to describe the constitutive relation of nanotwinned phase. The

strain-gradient plastic model is also presented to simulate the stress-strain relation of nano/ultrafine grained phase. In the framework of composite model, the contribution of microcracks generating during plastic deformation is taken into account in the mechanical properties of the bimodal nanotwinned composite. The calculations demonstrate that our proposed theoretical model can completely characterize the mechanical properties such as the yield strength, strain hardening, and elongation in such kind bimodal nanotwinned metal. These properties are sensitive to the microstructural size such as the twin spacing and grain size, as well as the volume fraction of each component.

2. Theoretical description

2.1 Composite model

Experiments have demonstrated that the bulk nanostructured austenitic stainless steel contains nano-sized/coarse grains with the nanoscale nanotwins embeded in micro-size grains by means of dynamic plastic deformation [30,32]. This complex microstructure can be characterized by a composite structure with a bimodal distribution of microstructures. This nanotwinned composite metal consists of polycrystalline phase and nanotwinned phase, as shown in figure 1. Motivated by this observation, we can consider the grain size in polycrystalline phase and twin spacing in nanotwinned phase as the bimodal size distribution in such nanotwinned composite metals. As a consequence, a modified mean-field approach is applied to simulate the stress-strain response of the bimodal nanotwinned metals, and the influence of bimodal size distribution must be taken into account. From the micromechanical model developed by Weng [55,56], the relationship between the hydrostatic and deviatoric strains of the constituent phases and those of the composite follows

$$\begin{aligned}
\varepsilon_{kk}^{(0)} &= \frac{\alpha_0^s(\kappa_1-\kappa_0)+\kappa_0}{c_0\alpha_0^s(\kappa_1-\kappa_0)+\kappa_0}\bar{\varepsilon}_{kk},\ \varepsilon_{ij}^{(0)\prime} = \frac{\beta_0^s(\mu_1-\mu_0^s)}{c_0\beta_0^s(\mu_1-\mu_0^s)+\mu_0^s}\bar{\varepsilon}_{ij}' - \frac{c_1\beta_0^s\mu_1}{c_0\beta_0^s(\mu_1-\mu_0^s)+\mu_0^s}\varepsilon_{ij}^{p(1)} \\
\varepsilon_{kk}^{(1)} &= \frac{\kappa_0}{c_0\alpha_0^s(\kappa_1-\kappa_0)+\kappa_0}\bar{\varepsilon}_{kk},\ \varepsilon_{ij}^{(1)\prime} = \frac{\mu_0^s}{c_0\beta_0^s(\mu_1-\mu_0^s)+\mu_0^s}\bar{\varepsilon}_{ij}' + \frac{c_0\beta_0^s\mu_1}{c_0\beta_0^s(\mu_1-\mu_0^s)+\mu_0^s}\varepsilon_{ij}^{p(1)}
\end{aligned}, \quad (1)$$

and the mean stress components of polycrystalline phase and nanotwinned phase are given by

$$\sigma_{kk}^{(1)} = 3\kappa_0 \frac{\kappa_1}{c_0\alpha_0^s(\kappa_1-\kappa_0)+\kappa_0}\bar{\varepsilon}_{kk}, \sigma_{ij}^{(1)\prime} = \frac{2\mu_0^s\mu_1[\bar{\varepsilon}_{ij}' - (1-c_0\beta_0^s)\varepsilon_{ij}^{p(1)}]}{c_0\beta_0^s(\mu_1-\mu_0^s)+\mu_0^s}$$
$$\sigma_{kk}^{(0)} = 3\kappa_0 \frac{\alpha_0^s(\kappa_1-\kappa_0)+\kappa_0}{c_0\alpha_0^s(\kappa_1-\kappa_0)+\kappa_0}\bar{\varepsilon}_{kk}, \sigma_{ij}^{(0)\prime} = \frac{2\mu_0^s\{[\beta_0^s(\mu_1-\mu_0^s)+\mu_0^s]\bar{\varepsilon}_{ij}' - c_1\beta_0^s\mu_1\varepsilon_{ij}^{p(1)}\}}{c_0\beta_0^s(\mu_1-\mu_0^s)+\mu_0^s} \quad (2)$$

Therefore, the dilatational and deviatoric stresses and strains of the composite are connected by

$$\bar{\sigma}_{kk} = 3\kappa_0\left[1+\frac{c_1(\kappa_1-\kappa_0)}{c_0\alpha_0^s(\kappa_1-\kappa_0)+\kappa_0}\right]\bar{\varepsilon}_{kk},$$
$$\bar{\sigma}_{ij}' = 2\mu_0^s\left\{\left[1+\frac{c_1(\mu_1-\mu_0^s)}{c_0\beta_0^s(\mu_1-\mu_0^s)+\mu_0^s}\right]\bar{\varepsilon}_{ij}' - \frac{c_1\mu_1}{c_0\beta_0^s(\mu_1-\mu_0^s)+\mu_0^s}\varepsilon_{ij}^{p(1)}\right\} \quad (3)$$

Here, $c_i (i = P,T)$ is the volume fraction of the polycrystalline phase or nanotwinned phase. *P* indicates the polycrystalline phase, and *T* represents the nanotwinned phase. α_S^s and β_S^s are the components of Eshelby's tensor for spherical inclusions, i.e.,

$$S_0^s = (\alpha_0^s, \beta_0^s), with\ \alpha_0^s = \frac{1+v_0^s}{3(1-v_0^s)}, \beta_0^s = \frac{2(4-5v_0^s)}{15(1-v_0^s)}. \quad (4)$$

The corresponding secant bulk and shear moduli of the *i*th phase are taken to satisfy the isotropic relations as follows

$$\kappa_i = \frac{E_i^s}{3(1-2v_i^s)}, \mu_i = \frac{E_i^s}{2(1+v_i^s)}, \quad (5)$$

in which the related secant Young's modulus and secant Poisson ratio of *i*th phase is written as

$$E_i^s = \frac{\sigma_i}{\varepsilon_i^e+\varepsilon_i^p} = \frac{E_i}{1+\frac{E_i\varepsilon_i}{\sigma_{flow}^i}(\frac{\sigma_{i11}}{\sigma_{flow}^i})^{m_0-1}}, \quad v_i^s = \frac{1}{2}-(\frac{1}{2}-v_i\frac{E_i^s}{E_i}). \quad (6)$$

Here, E_i and v_i denote the Young's modulus and Poisson's ratio of the *i*th phase. The flow stress σ_{flow}^i for polycrystalline phase and nanotwinned phase will be presented in the next section.

2.2 Constitutive relations

To grasp the overall stress-strain response of bimodal nanotwinned composite by using the micromechanical model, the constitutive relations of the polycrystalline

phase and nanotwinned phase in composite structures must be identified. Here, the mechanism-based strain gradient plasticity [57] is adopted to describe the stress-strain response for the constituents in bimodal nanotwinned composite. The strain rate $\dot{\boldsymbol{\varepsilon}}$ can be decomposed into its elastic and plastic parts,

$$\dot{\boldsymbol{\varepsilon}} = \dot{\boldsymbol{\varepsilon}}^{\mathbf{e}} + \dot{\boldsymbol{\varepsilon}}^{\mathbf{p}}. \tag{7}$$

The elastic strain rate is obtained from the stress rate in the linear elastic relation as

$$\dot{\boldsymbol{\varepsilon}}^{\mathbf{e}} = \mathbf{M} : \dot{\boldsymbol{\sigma}}, \tag{8}$$

where $\mathbf{M}$ is the elastic compliance tensor. The plastic strain rate is proportional to the deviatoric stress $\boldsymbol{\sigma}'$ based on the conventional J_2-flow theory of plasticity, given as

$$\dot{\boldsymbol{\varepsilon}}^{\mathrm{p}} = \frac{3\dot{\varepsilon}^{\mathrm{p}}}{2\sigma_{\mathrm{e}}}\boldsymbol{\sigma}', \tag{9}$$

where $\sigma'_{ij} = \sigma_{ij} - \sigma_{kk}\delta_{ij}/3$ and $\sigma_e = \sqrt{3\sigma'_{ij}\sigma'_{ij}/2}$ is the von Mises equivalent stress. $\dot{\varepsilon}^{\mathrm{p}}$ is the equivalent plastic strain rate, expressed as

$$\dot{\varepsilon}^{\mathrm{p}} = \dot{\varepsilon}\left[\frac{\sigma_{\mathrm{e}}}{\sigma_{flow}}\right]^{\mathrm{m}_0}, \tag{10}$$

where $\dot{\varepsilon} = \sqrt{2\dot{\varepsilon}'_{ij}\dot{\varepsilon}'_{ij}/3}$ is the equivalent strain rate and $\dot{\varepsilon}'_{ij} = \dot{\varepsilon}_{ij} - \dot{\varepsilon}_{kk}\delta_{ij}/3$. m_0 is the rate-sensitivity exponent and σ_{flow} is the flow stress. Since the deformation mechanism in nano-grained/coarse-grained phase is quite different with the one in nanotwinned phase, the flow stresses in polycrystalline phase and nanotwinned need to be addressed separately.

2.2.1 Nanotwinned phase

The nano-scale twin lamellae in nanotwinned metals with a composite structure play an important role in strengthening the materials. The nanotwinned phase not only acts as the harder phase but also keep a good plasticity. The twin boundaries, similar to the grain boundaries, enable to provide more obstacles during dislocation motion. Here, the dislocation density in the areas of dislocation pile-up nearby the twin boundaries is present to describe the influence of the twin boundaries on the flow

stress. Therefore, a generalized Taylor relation of flow stress in the nanotwinned phase tells

$$\sigma_{flow} = \sigma_0 + M\alpha\mu b\sqrt{\rho_I + \rho_{TB}}\,, \tag{11}$$

where α, μ, b and M are the empirical constant, the shear modulus, the Burger constant and the Taylor factor, respectively. σ_0 is the lattice friction stress. ρ_{TB} is the dislocation density in the dislocation pile-up zones nearby the twin boundaries and can be expressed as [51,58]

$$\rho_{TB} = \phi^{TB}\left(\frac{12N_0}{\pi d_G^{T2}} + \frac{12n_p'}{\sqrt{3}\pi d_G^{T}} d_{TB}^{-1}\right) - \frac{3\phi_0}{\sqrt{3}} d_{TB}^{-2}\,, \tag{12}$$

where d_G^{T} is the size of grains with the twin lamellae, n_p' is the number of initial partial dislocations and N_0 is the maximum number of full dislocations in grain, both of which are independent of the twin spacing. ϕ_0 and ϕ^{TB} are the geometrical parameters. ρ_{I} denotes the density of dislocations in the crystal interior of grains, which can be derived from Kocks and Mecking's model [59,60], i.e.,

$$\frac{\partial\rho_I}{\partial\varepsilon^{\mathrm{p}}} = M\left(\frac{k}{d_G^{T}} + k_1\sqrt{\rho_I} - k_2\rho_I\right). \tag{13}$$

Here, $k = 1/b; k_1 = \psi/b; k_2 = k_{20}(\dot{\varepsilon}^{\mathrm{p}}/\dot{\varepsilon}_0)^{-1/\mathrm{n}_0}$, ψ is a proportionality factor, k_{20} and $\dot{\varepsilon}_0$ are the constants, and n_0 is inversely proportional to the temperature. ε^{p} is the plastic strain. Note that the althermal storage of dislocations and the annihilation of dislocations during the dynamic process are both involved in the K-M model.

2.2.2 Polycrystalline phase

The experimental studies showed that the nanograins can be generated during DPD process, and the annealing process makes the nanograins grow into micrometer-scale grains [29,31]. Thereby, the grain size in polycrystalline phase can be ranged from several tens of nanometer to several micrometers or even larger. From this perspective, we should present the flow stresses of nano-grains and coarse-grains separately.

When the grain size in the polycrystalline phase is in the nanometer-scale, the strength of the nano-grained phase will be reinforced significantly. This is originated from the increased grain boundaries blocking the motion of more lattice dislocations. Thereby, the effects of grain boundaries are taken into account during plastic deformation in the nano-grained phase. The dislocation density in the grain boundary dislocation pile-up zones (GBDPZs) is addressed to characterize the contribution of grain boundaries on the flow stress, expressed as [20]

$$\sigma_{flow}^{\mathrm{N}} = \sigma_0 + M\alpha\mu b\sqrt{\rho_I + \rho_{GB}}\,, \tag{14}$$

where ρ_{GB} and ρ_I are the density of dislocation in the dislocation pile-up zones nearby grain boundaries and the one in the crystal interior, respectively. ρ_I can be determined from Eq. (13). ρ_{GB} is the density of dislocations in the GBDPZ , given by [51]

$$\rho_{GB} = \frac{n^{GB}\lambda^{GB}}{V_{Cell}} = k^{GB}\frac{\eta^{GB}}{b}\,, \tag{15}$$

where $k^{GB} = 6d_{GBDPZ}/\phi^{GB}d_G$, d_{GBDPZ} is the thickness of GBDPZ, d_G is the grain size in polycrystalline phase without twins. n^{GB} is the number of dislocations around the grain boundaries and ϕ_3 is the geometrical factor. $\lambda \approx \pi d_G$ is the average length of the dislocation loop for dislocations in the GBDPZ.

Due to the fact that the primary deformation mechanism in the coarse-grained phase is dominated by the intragrain dislocation-mediated interaction, and the Taylor-type relationship can be utilized to describe the flow stress which is related to the dislocation density. Therefore, the flow stress of the coarse-grained phase can be expressed as:

$$\sigma_{flow}^{\mathrm{C}} = \sigma_0 + M\alpha\mu b\sqrt{\rho_I} + \sigma_{\mathrm{b}}\,, \tag{16}$$

where σ_b represents the back stress. Note that the Taylor evolution law contains the isotropic strain-hardening and the back-stress-induced kinematic hardening. The back stress term in Eq. (16) can be expressed by

$$\sigma_b = M\frac{\mu b}{d_G}N_{\mathrm{b}}, \tag{17}$$

where N_{b} is the number of dislocations blocked at the grain boundaries of the coarse grain phase, which depends on the plastic strain following the evolution law [61,62],

$$\frac{dN_{\mathrm{b}}}{d\varepsilon^{\mathrm{p}}} = \frac{\zeta}{b}(1-\frac{N_{\mathrm{b}}}{N_0^{\mathrm{b}}}). \tag{18}$$

Here, ζ and N_0^{b} are the mean spacing between slip bands and the maximum number of dislocation loops at the grain boundary in the coarse-grained metal, respectively.

2.3 Contributions of microcracks

For the bimodal nanostructured metals, the nanovoids or nano/microcracks can be induced during plastic deformation in the matrix of nano-grained or ultrafine grained phase, as shown in figure 2. These nanoscale voids/cracks will affect the mechanical properties of bimodal metals significantly through modifying the stress states around the voids/cracks and the constitutive relation in the matrix phase. In the nanotwinned metals with bimodal distribution of microstructural size, the appearance of nano/microcracks in the matrix phase results in the change of overall stress and strain of polycrystalline phase. The microcrack-matrix-effective-medium approach can be utilized to model the stress and strain in the matrix phase of bimodal nanotwinned metals. Suppose the representative volume element (RVE) boundary is subjected to tractions in equilibrium with a uniform overall stress of σ^{∞}. The average strain in a solid with nano/microcracks is consistent with regular and singular parts as

$$\bar{\boldsymbol{\varepsilon}} = \bar{\boldsymbol{\varepsilon}}^{\mathbf{m}} + \bar{\boldsymbol{\varepsilon}}^{\mathbf{c}}, \tag{19}$$

where $\bar{\boldsymbol{\varepsilon}}^{\mathbf{m}}$ is the matrix strain averaged over the RVE and $\bar{\boldsymbol{\varepsilon}}^{\mathbf{c}}$ is the nano/microcrack-induced variations in the overall average strain, respectively. When the matrix deform in the elastic region, the matrix strain can be written as $\bar{\boldsymbol{\varepsilon}}^{\mathbf{m}} = \mathbf{M}^{\mathbf{m}} : \boldsymbol{\sigma}^{\infty}$. Since the nano/microcracks generated during the plastic deformation are supposed to be parallel, the corresponding effective moduli are as follows:

$$E_1 = E_0[1+\frac{16(1-\nu_0^2)}{3}\rho]^{-1}; G_{12} = G_0[1+\frac{8(1+\nu_0)}{3(1-\nu_0/2)}\rho]^{-1}. \quad (20)$$

It should be noted from Eq. (20) that the effective moduli of the bimodal nanotwinned metals are associated with the density of microcracks in the materials. The number of these cracks will be increased during the plastic deformation, leading to that the density of nano/microcracks in the bimodal nanotwinned metals is sensitive to the applied stress or strain. From this perspective, the strain-based Weibull distribution function with respect to the plastic strain is applied to character the number of cracks. Thereby, the density of nano/microcracks can be expressed as

$$\rho = \rho_0(1-f_W(\varepsilon_p)) = \rho_0[1-\exp(-(\varepsilon_p/\varepsilon_0)^{\mathrm{M}}] \quad (21)$$

Here, ρ_0 is a constant; $f_W(\varepsilon_p)$ is the strain-based Weibull distribution function in which ε_0 is the reference strain and M is the Weibull modulus. On the other hand, the existence of nano/microcracks indicates that the number of dislocations blocked at the grain boundaries or around the cracks is increased. These dislocations pile-up along the grain boundaries will lead to back stress effects on the strain hardening which must be taken into account during the plastic deformation in the nano/ultrafine-grained phase. Therefore, the constitutive relation of the nano-grained phase will contain the back stress term in the flow stress expression, which is changed into

$$\sigma_{flow} = \sigma_0 + M\alpha\mu b\sqrt{\rho_I + \rho_G} + \sigma_b^*, \quad (22)$$

where σ_b^* is the nano/microcrack-induced back stress.

3. Results and discussion

We use the 316L austenitic stainless steel (316Lss) as an illustrative example to explore the relationship between mechanical properties and the size and volume fraction of microstructures in nanotwinned metals with a composite structure. A set of material parameters for 316Lss used in our simulations is extracted from the literature or fit with the experimental data [29-32], as listed in Table 1. Since the effective thickness of the TBDPZ and GBDPZ is supposed to range from 7 to 10 lattice parameters [48], we chose d_{GBDPZ} and d_{TBDPZ} of stainless steel around 3.6 nm. Under these parameters, the yield strength and ductility in the bimodal nanotwinned

316Lss are simulated based on the proposed model. Figure 3 plots the simulated stress-strain responses for the coarse-grained 316Lss and bimodal nanotwinned 316Lss with various microstructural scales. The corresponding experimental measurements for bimodal nanotwinned 316Lss with different annealing temperature are also reproduced in the figure. It is noted from the figure that the proposed micromechanical model can describe the mechanical properties of bimodal nanotwinned 316Lss successfully. The simulations agree well with the experimental data, including the yield strength, strain hardening, and uniform elongation, for different bimodal nanotwinned samples with annealing temperature of 730°C, 750°C, and 770°C. It means that the proposed model can be applicable to predict the mechanical properties of bimodal nanotwinned 316Lss for different volume fractions of components and different sizes of microstructures.

Experimental studies demonstrated that the work-hardening rate of bimodal nanotwinned 316Lss is quite sensitive to the annealing temperature [31, 32]. We plot the simulated work-hardening rate ($\Theta=d\sigma/d\varepsilon$) as a function of applied true strain in figure 4(a) for various microstructural scales and volume fractions. The experimental data are also provided in the figure 4(b). From figure 4(a), it can be noticed that all curves of work-hardening rates for bimodal nanotwinned 316Lss intersect the curve of the as-received coarse-grained 316Lss. It means that with the applied strain increasing, the work-hardening rates of bimodal nanotwinned 316Lss are larger than that of the as-received coarse-grained specimens until the applied strain reaches the intersection point, and then the bimodal nanotwinned samples has a lower strain hardening rate. We can also find from figures 4(a) and 4(b) that the predictions for work-hardening rate are consistent with the experimental data. On the other hand, one can learn from figure 4(a) that the simulated work-hardening rate in the bimodal nanotwinned 316Lss decreases with the applied strain increasing, which is in accordance with experimental observations [31]. In the present model, the influences of the nano/microcracks are taken into account on plastic deformation in the bimodal nanotwinned stainless steels. These nano/microcracks could be generated in the polycrystalline phase and blocked by the nanotwin bundles, giving rise to more nano/microcracks appearing in polycrystalline matrix phase with further deformation.

Since the occurrence of nano/microcracks enables to change the stress and strain in the polycrystalline matrix phase, the nano/microcrack-induced strain will increase with the density of nano/microcrack increasing, leading to the decrease of effective strain in the polycrystalline matrix phase. As a result, the effects of the back stress in the polycrystalline matrix phase which provides the kinetic strain hardening, become faded with further deformation. Alternatively, the work-hardening rate decreases with applied strain increasing.

The contribution of the nano/microcracks on the mechanical properties in bimodal nanotwinned metals are taken into account in the proposed model, leading to the stress-strain relation in the matrix phase related to the density of microcracks. Since the Weibull distribution function is involved to describe the density of microcacks as a function of plastic strain, the simulated results are associated with the parameters in the function of microcracks density. Figure 5 shows the simulated results for the bimmodal nanotwinned 316Lss with different reference density of microcracks ρ_0. One can note from figure 5(a) that the failure strain is sensitive to the reference density of microcracks. The larger the reference density is, the smaller the failure strain is. We can find it more clearly in figure 5(b) that the failure strain decreases with the reference density nonlinearly. Figure 6 further depicts the influence of the Weibull modulus in Weibull distribtuion function on the mechanical properties of bimodal nanotwinned 316Lss. It can be clearly noticed that the more pronounced plasticity can be reached for the larger Weibull modulus, as shown in figure 6(a). We also can note that the failure strain varies with the Weibull modulus nonlinearly. From figures 5 and 6, interesting noted is that the various parameters in the function of microcracks density can induce to the change of only the failure strain but not the yield strength.

Being analogous to traditional composite structure, the mechanical performance of bimodal nanotwinned composite metals is closely related to the volume faction of components. Figure 7(a) shows stress-strain relation for bimodal nanotwinned 316Lss with different volume fraction of nanotwinned phase. From the figure, clearly noted is that the yield strength is improved significantly with increasing the volume fraction f_{TW}. For example, the yield strength is enhanced from 400 MPa to 800 MPa with

f_{TW} changed from 0.1 to 0.5. In addition, the failure strain of bimodal nanotwinned 316Lss is also relevant to the volume fraction of nanotwinned phase. Figure 7(b) plots the strength varied with the failure strain for different volume fraction. With increasing the volume fraction, the yield strength and ultimate strength are both increased with the failure strain decreased. The variation of yield strength is more prominent than that of ultimate strength.

Due to the fact that the predicted stress-strain responses of bimodal nanotwinned 316Lss are pronouncedly dependent on the volume fraction of nanotwinned phase and the Weibull modulus in distribution function of nano/microcrack as shown in figures. 6 and 7, we depict the work-hardening rate of bimodal nanotwinned 316Lss with different f_{TW} and various Weibull modulus M in figures 8(a) and 8(b), respectively. It can be found from figure 8(a) that the work-hardening rate of bimodal nanotwinned 316Lss is decreased with the volume fraction of nanotwinned phase increasing. With the larger volume fraction f_{TW}, the work-hardening rate decreases sharply with strain after elastic deformation, and then turns into approximately linear change with further increasing the strain. It is because that the increasing volume fraction of nanotwinned phase weakens the kinematic strain hardening originated from back stress in the polycrystalline phase, leading to the lower work-hardening rate for larger volume fraction of nanotwinned phase. From figure 8(b), we can further note that the work-hardening rate is related to the Weibull modulus. With the Weibull modulus decreasing from 10 to 2, the work-hardening capability gradually exhausted in the bimodal nanotwinned 316Lss.

On the basis of micromechanical model presented in section 2, one can note that the constitutive relation of nanotwinned phase involves the feature sizes of microstructures such as the twin spacing and grain size. Therefore, the total stress-strain response of the bimodal nanotwinned composite is sensitive to the size of twin lamellae. Figure 9(a) shows the curves of stress-strain relation of bimodal nanotwinned 316Lss with different twin spacing in nanotwinned phase. One can find that both the yield strength and ultimate strength are enhanced with the size of twin lamellae decreasing. We further plot the relationship between the strength and the failure strain for different twin spacings in figure 9(b). With twin spacing decreasing,

both the strength and failure strain are improved. From figures (7) and (9), it can be concluded that the combination performance of strength and ductility in bimodal nanotwinned metals can be controlled by tuning the volume fraction of components and feature sizes of microstructures.

4. Conclusion

In summary, a theoretical model incorporating multiple strengthening mechanisms is proposed to explore the strength and ductility of the nanotwinned metals with composite structures. The modified mean-field approach is utilized to calculate the total stress-strain relationship in which the constitutive models of nano/ultrafine grained phase and the nanotwinned phase are involved. The contribution of nano/microcracks in the bimodal nanotwinned metals are taken into account to study strain hardening and failure strain. The numerical results indicate that the proposed model can describe mechanical properties of the bimodal nanotwinned metals successfully. The predictions agree well with their experimental results. Moreover, the detailed simulations show that the mechanical properties of nanotwinned metals with composite structures are significantly dependent on the twin spacing and the volume fraction of nanotwinned phase. The present work will provide a theoretical framework to design the yield strength and ductility of nanotwinned metals with composite structures by controlling volume fraction of components and microstructural feature size.

Acknowledgements

The authors gratefully acknowledge the support from the National Natural Science Foundation of China (Grant nos. 11472243, 11302189, 11321202, 11102128 and 11372214), and Doctoral Fund of Ministry of Education of China (20130101120175), the National Basic Research Program of China under the grant 2012CB932203 and 2015CB856800, the Hong Kong government through the General Research Fund with grants GRF/CityU519110, the Croucher Fundation CityU9500006, the Early Career Scheme (ECS) of Hong Kong RGC (Grant No. 25200515) and the Departmental General Research Fund (G-UA2L) from the Hong Kong Polytechnic University.

References

[1] Weertman JR, Farkas D, Hemker K, Kung H, Mayo M, Mitra R, Van Swygenhoven H. Structure and mechanical behavior of bulk nanocrystalline materials. Mater Res Soc Bull 1999; 24(2): 44-50.

[2] Kumar KS, Van Swygenhoven H, Suresh, S. Mechanical behavior of nanocrystalline metals and alloys. Acta Mater 2003; 51(19): 5743-74.

[3] Meyers MA, Mishra A, Benson DJ. Mechanical properties of nanocrystalline materials. Prog Mater Sci 2006; 51(4): 427-556.

[4] Dao M, Lu L, Asaro RJ, De Hosson JTM, Ma E. Toward a quantitative understanding of mechanical behavior of nanocrystalline metals. Acta Mater 2007; 55(12): 4041-65.

[5] Gibson RF. A review of recent research on mechanics of multifunctional composite materials and structures. Compos Struct 2010; 92(12): 2793-810.

[6] Zhu T, Li J. Ultra-strength materials. Prog Mater Sci 2010; 55(7): 710-57.

[7] Suryanarayana C. Mehcanical behavior of emerging materials. Mater Today 2012; 15(11):486-96.

[8] Lu L, Shen YF, Chen XH, Qian LH, Lu K. Ultrahigh strength and high electrical conductivity in copper. Science 2004; 304(5669): 422-6.

[9] Zhu YT, Liao XZ. Nanostructured metals: retaining ductility. Nat Mater 2004; 3(6): 351-2.

[10] Yamakov V, Wolf D, Phillpot SR, Mukherjee AK, Gleiter H. Deformation mechanism map for nanocrystalline metals by molecular dynamics simulation. Nature Mater 2004; 3(1):43-7.

[11] Ritchie RO. The conflicts between strength and toughness. Nat Mater 2011; 10(11): 817-22.

[12] Bouaziz O, Allain S, Scott CP, Cugy P, Barbier D. High manganese austenitic twinning induced plasticity steels: A review of the microstructure properties relationships. Curr Opin Solid State Mat Sci 2011; 15(4): 141-68.

[13] Kou HN, Lu J, Li Y. High-strength and high-ductility nanostructured and amorphous metallic materials. Adv Mater 2014; 26(31):5518-24.

[14] Tellkamp VL, Melmed A, Lavernia EJ. Mechanical behavior and microstructure of a thermally stable bulk nanostructured Al alloy. Metall Mater Trans A 2001; 32(9): 2335-43.

[15] Wang YM, Chen MW, Zhou FH, Ma E. Extraordinarily high tensile ductility in a nanostructured metal. Nature 2002; 419(6910): 912-5.

[16] Zhao YH, Topping T, Bingert JF, Thornton JJ, et al. High tensile ductility and strength in bulk nanostructured nickel. Adv Mater 2008; 20(16): 3028-33.

[17] Li YS, Zhang Y, Tao NR, Lu K. Effect of thermal annealing on mechanical properties of a nanostructured copper prepared by means of dynamic plastic deformation. Scripta Mater 2008; 59(4): 475-8.

[18] Dirras G, Gubicza J, Bui QH, Szilagyi T. Microstructure and mechanical characteristics of bulk polycrystalline Ni consolidated from blends of powders with different particle size. Mater Sci Eng A 2010; 527(4-5): 1206-14.

[19] Zhu LL, Lu J. Modelling the plastic deformation of nanostructured metals with bimodal grain size distribution. Int J Plast 2012; 30-31: 166-84.

[20] Zhu LL, Shi SQ, Lu K, Lu J. A statistical model for predicting the mechanical properties of nanostructured metals with bimodal grain size distribution. Acta Mater 2012; 60(16):5762-72.

[21] Guo X, Ji R, Weng GJ, Zhu LL, Lu J. Micromechanical simulation of fracture behavior of bimodal nanostructured metals. Mater Sci Eng A 2014; 618: 479-89.

[22] Guo X, Dai XY, Weng GJ, Zhu LL, Lu J. Numerical investigation of fracture behavior of nanostructured Cu with bimodal grain size distribution. Acta Mech 2014; 225(4): 1093-106.

[23] Shen MJ, Zhang BH, Wang XJ, Zhang MF, Zheng MY, Wu K. Significantly improved strength and ductility in bimodal-size grained microstructural magnesium matrix composites reinforced by bimodal sized SiCp over traditional magnesium matrix composites. Comp Sci Tech 2015; doi:10.1016/j.compscitech.2015.08.009.

[24] Lu L, Shen YF, Chen XH, Qian LH, Lu K. Ultrahigh strength and high electrical conductivity in copper. Science 2004; 304(5669): 422-6.

[25] Lu L, Chen X, Huang X, Lu K. Revealing the maximum strength in nano-twinned copper. Science 2009; 323(5914): 607-10.

[26] Lu K, Lu L, Suresh S. Strengthening materials by engineering coherent internal boundaries at the nanoscale. Science 2009; 324(5925): 349-52.

[27] Chen AY, Ruan HH, Wang J, Chan HL, Wang Q, Li Q, Lu J. The influence of strain rate on the microstructure transition of 304 stainless steel. Acta Mater 2011; 59(9):3697-709.

[28] Chen AY, Li DF, Zhang JB, Song HW, Lu J. Make nanostructured metal exceptionally tough by introducing non-localized fracture behaviors. Scripta Mater 2008; 59(6):579-82.

[29] Lu K, Yan FK, Wang HT, Tao NR. Strengthening austenitic steels by using nanotwinned austenitic grains. Scripta Mater 2012; 66 (11); 878-83.

[30] Wang HT, Tao NR, Lu K. Strengthening and austenitic Fe-Mn steel using nanotwinned austenitic grains. Acta Mater 2012; 60 (9): 4027-40.

[31] Yan FK, Liu GZ, Tao NR, Lu K. Strength and ductility of 316L austenitic stainless steel strengthened by nano-scale twin bundles. Acta Mater 2012; 60 (3): 1059-71.

[32] Yan FK, Tao NR, Archie F, Gutierrez-Urrutia I, Raabe D, Lu K. Deformation mechanisms in an austenitic single-phase duplex microstructured steel with nanotwinned grains. Acta Mater 2014; 81: 487-500.

[33] Zhang F, Lisle T, Curtin WA, Xia Z. Multiscale modeling of ductile-fiber-reinforced composites. Comp Sci Tech 2009; 69(11-12): 1887-1895.

[34] Orlik J. Asymptotic homogenization algorithm for reinforced metal-matrix elasto-plastic composites. Compos Struct 2010; 92(7):1581-901.

[35] Barera O, Cocks ACF, Ponter ARS. The linear matching method applied to composite materials: A micromechanical approach. Comp Sci Tech 2011; 71(6): 797-804.

[36] Stig F, Hallstrom S. A modelling framework for composites containing 3D reinforcement. Compos Struct 2012; 94(9):2895-901.

[37] Song SN, Chen Y, Su ZC, Quan CG, Tan VBC. Multiscale modeling of damage progression in nylon 6/clay nanocomposite. Comp Sci Tech 2014; 100: 189-197.

[38] Guo X, Ji R, Weng GJ, Zhu LL, Lu J. Computer simulation of strength and ductility of nanotwin-strengthened coarse-grained metals. Modelling Simul Mater Sci Eng 2014; 22(7): 075014.

[39] Joshi SP, Ramesh KT, Han BQ, Lavernia EJ. Modeling the constitutive response of bimodal metals. Metall. Mater. Trans. A 2006; 37(8): 2397-404.

[40] Berbenni S, Favier V, Berveiller M. Impact of the grain size distribution on the yield stress of heterogeneous materials. Int J Plasticity 2007; 23(1): 114-42.

[41] Ramtani S, Dirras G, Bui HQ. A bimodal bulk ultra-fine-grained nickel: experimental and micromechanical investigations. Mech Mater 2010; 42(5): 522-36.

[42] Froseth A, Derlet PM, Van Swygenhoven H. Grown-in twin boundaries affecting deformation mechanisms in nc-metals. Appl Phys Lett 2004; 85(24): 5863-5.

[43] Wang J, Huang H. Novel deformation mechanism of twinned nanowires. Appl Phys Lett 2006; 88(20): 203112.

[44] Afanasyev KA, Sansoz F. Strengthening in gold nanopillars with nanoscale twins. Nano Lett 2007; 7(7): 2056-62.

[45] Zhu T, Li J, Samanta A, Kim HG, Suresh S. Interfacial plasticity governs strain rate sensitivity and ductility in nanostructured metals. Proc Natl Acad Sci 2007, 104(9): 3031-6.

[46] Li XY, Wei YJ, Lu L, Lu K, Gao HJ. Dislocation nucleation governed softening and maximum strength in nano-twinned metals. Nature 2010; 464(7290): 877-80.

[47] You ZS, Li XY, Gui LG, Lu QH, Zhu T, Gao HJ, Lu L. Plastic anisotropy and associated deformation mechanisms in nanotwinned metals. Acta Mater 2013; 61(1): 217-27.

[48] Dao M, Lu L, Shen Y, Suresh, S. 2006. Strength, strain-rate sensitivity and ductility of copper with nanoscale twins. Acta Mater 2006; 54(20): 5421-32.

[49] Jerusalem A, Dao M, Suresh S, Radovitzky R 2008. Three-dimensional model of strength and ductility of polycrystalline copper containing nanoscale twins. Acta Mater 2008; 56(17): 4647-57.

[50] Mirkhani H, Joshi SP. 2011. Crystal plasticity of nanotwinned microstructures: A discrete twin approach for copper. Acta Mater 2011; 59(14): 5603-17.

[51] Zhu LL, Ruan HH, Li XY, Dao M, Gao HJ, Lu J. Modeling grain size dependent optimal twin spacing for achieving ultimate high strength and related high ductility in nanotwinned metals. Acta Mater 2011; 59(14): 5544-57.

[52] Wei YJ. Scaling of maximum strength with grain size in nanotwinned fcc metals. Phys. Rev. B 2011; 83: 132104.

[53] Gu P, Dao M, Asaro RJ, Suresh S. A unified mechanistic model for size-dependent deformation in nanocrystalline and nanotwinned metals. Acta Mater 2011; 59(18): 6861-8.

[54] Gu P, Dao M, Suresh S. Analysis of size-dependent slip transfer and inter-twin flow stress in a nanotwinned fcc metal. Acta Mater 2014; 67**:** 409-17.

[55] Weng GJ. The overall elastoplastic stress–strain relation of dual-phase metals. J Mech Phys Solid 1990; 38(3): 419-41.

[56] Weng GJ. A homogenization scheme for the plastic properties of nanocrystalline materials. Rev Adv Mater Sci 2009; 19: 41-62.

[57] Huang Y, Qu S, Hwang KC, Li M, Gao H. A conventional theory of mechanism-based strain gradient plasticity. Int J Plast 2004; 20(4-5): 753-82.

[58] Zhu LL, Qu SX, Guo X, Lu J. Analysis of the twin spacing and grain size effects on mechanical properties in hierarchically nanotwinned face-centered cubic metals based on a mechanism-based plasticity model. J Mech Phys Solid 2015; 76: 162-79.

[59] Kocks UF, Mecking H. The physics and phenomenology of strain hardening. Prog Mater Sci 2003; 48(3): 171-273.

[60] Capolungo L, Jochum C, Cherkaoui M, Qu J. Homogenization method for strength and inelastic behavior of nanocrystalline materials. Int J Plast 2005; 21: 67-82.

[61] Sinclair CW, Poole WJ, Bréchet Y. A model for the grain size dependent work hardening of copper. Scripta Mater 2006; 55(8): 739-42.

[62] Bouaziz O, Allain S, Scott C. Effect of grain and twin boundaries on the hardening mechanisms of twinning-induced plasticity steel. Scripta Mater 2008; 58(6): 484-7.

Figure captions

Figure 1. Schematic drawings of the bimodal nanotwinned metals in the polycrystalline materials with the assumption of the composite model

Figure 2. Schematic drawings of cracks arising during tensile testing

Figure 3. Comparison of the stress–strain relationship between the experimental results [31] and simulations for bimodal nanotwinned 316Lss and coarse-grained 316Lss. The coarse grain size is 2.35 μm. The size of

nanotwinned grain is around 5 μm with the twin spacing of 31 nm, 26 nm, and 26 nm for annealed temperature of 770°C, 750°C, and 730°C, respectively.

Figure 4. (a) The simulated work-hardening rate ($\Theta=d\sigma/d\varepsilon$) varied with true strain and (b) the experimental measurementsof strain-dependent work-hardening rate for nanotwinned samples for annealed temperature of 730°C,750°C and 770°C [31].

Figure 5. (a) Influence of the reference density of microcracks on the stress-strain response, (b) and the failure strain varied with the reference density ρ_0.

Figure 6. (a) Influence of the Weibull modulus on the stress-strain response and (b) the uniform elongation as the function of Weibull modulus M.

Figure 7. (a)Stress-strain response of nanotwinned composite with different volume fraction of the nanotwins and (b) the strength varied with the failure strain for different volume fraction of nanotwins.

Figure 8. The simulated work-hardening rate ($\Theta=d\sigma/d\varepsilon$) vs. (a) true strain for different voume fraction of nanotwinned phase and (b) various Weibull modulus.

Figure 9. (a) Stress-strain response of nanotwinned composite with different twin spacings and (b) strength and uniform elongation for various twin spacings.

Table 1

Description, symbol, and magnitude for the different parameters in the model

Parameter (Unit)	Symbol	Magnitude
Grain size (nm)	$d_G; d_G^T$	2380; 5000
Elastic modulus (GPa)	E	199.6
Shear modulus (GPa)	μ	86
Poisson's ratio	ν	0.29
Burgers vector (nm)	b	0.26
Taylor factor	M	3.06
Taylor constant	α	0.3
Thickness of GBDPZ (nm)	d_{GBDPZ}	3.6
Thickness of TBDPZ (nm)	d_{TBDPZ}	3.6
Maximum number of dislocation loops	N_0^{b}	500
Maximum number of dislocation	N_0	1090
Number of initial partial dislocation	n_p'	321
Geometrical parameter	ϕ_0	3.2
Dynamic recovery constant	k_{20}	18.5
Proportionality factor	ψ	0.2
Dynamic recovery constant	n	12.25
Reference strain rate (s^{-1})	$\dot{\varepsilon}_0$	1.75
Geometric factor	$\phi^{TB}, \phi_i (i = 1, 2)$	0.5~1.5

Figure1

Click here to download high resolution image

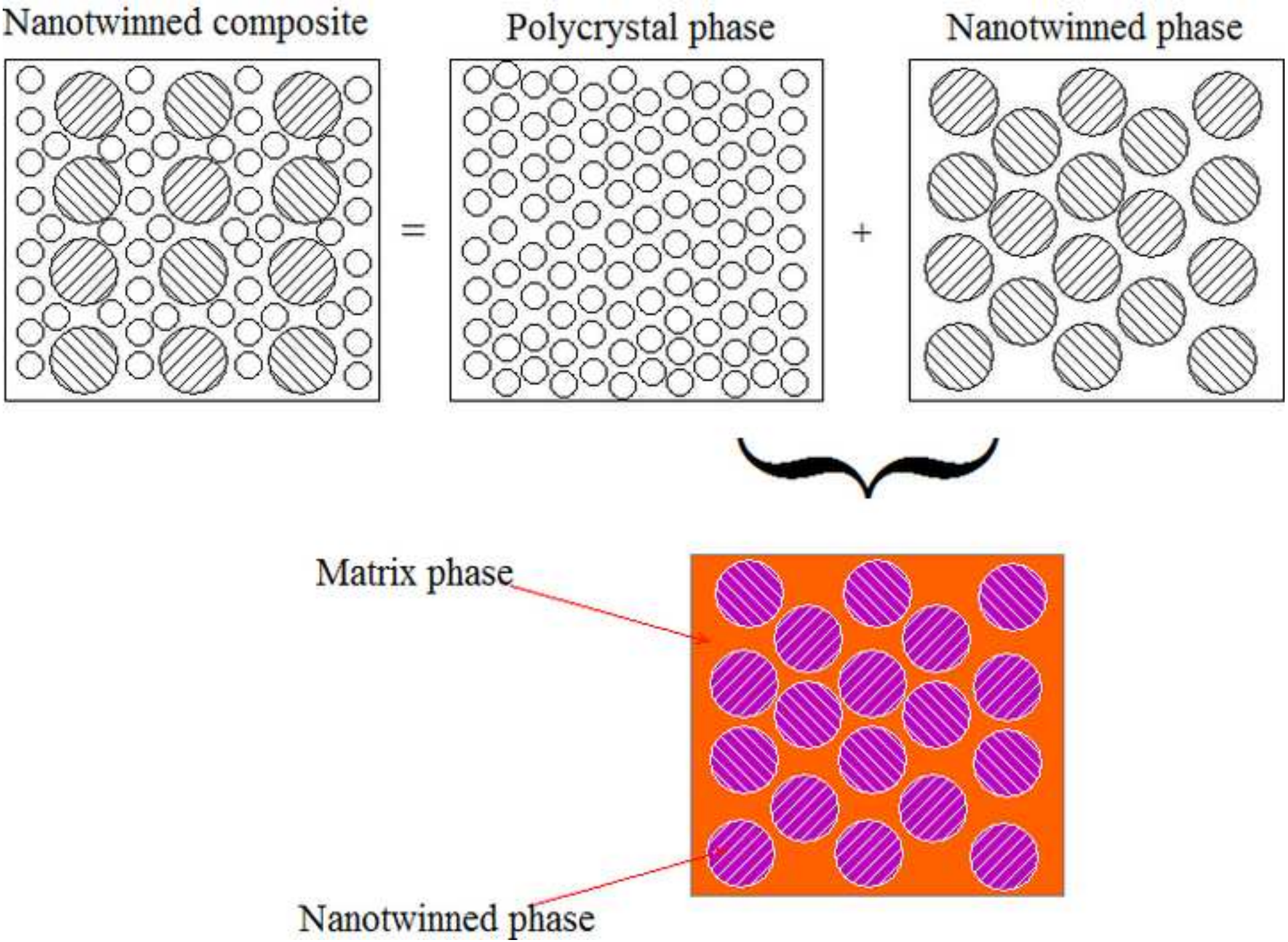

Figure2

Click here to download high resolution image

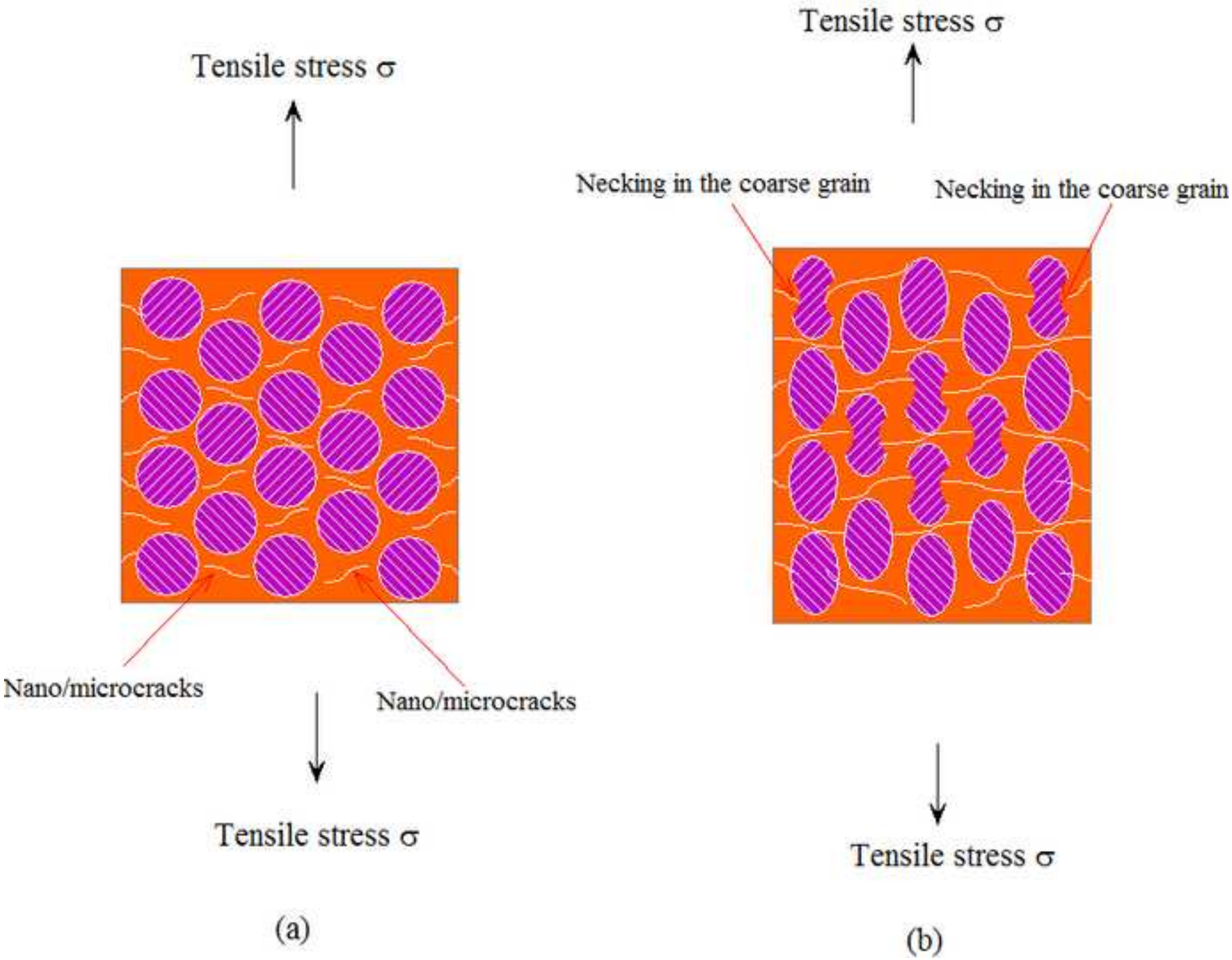

Figure3
Click here to download high resolution image

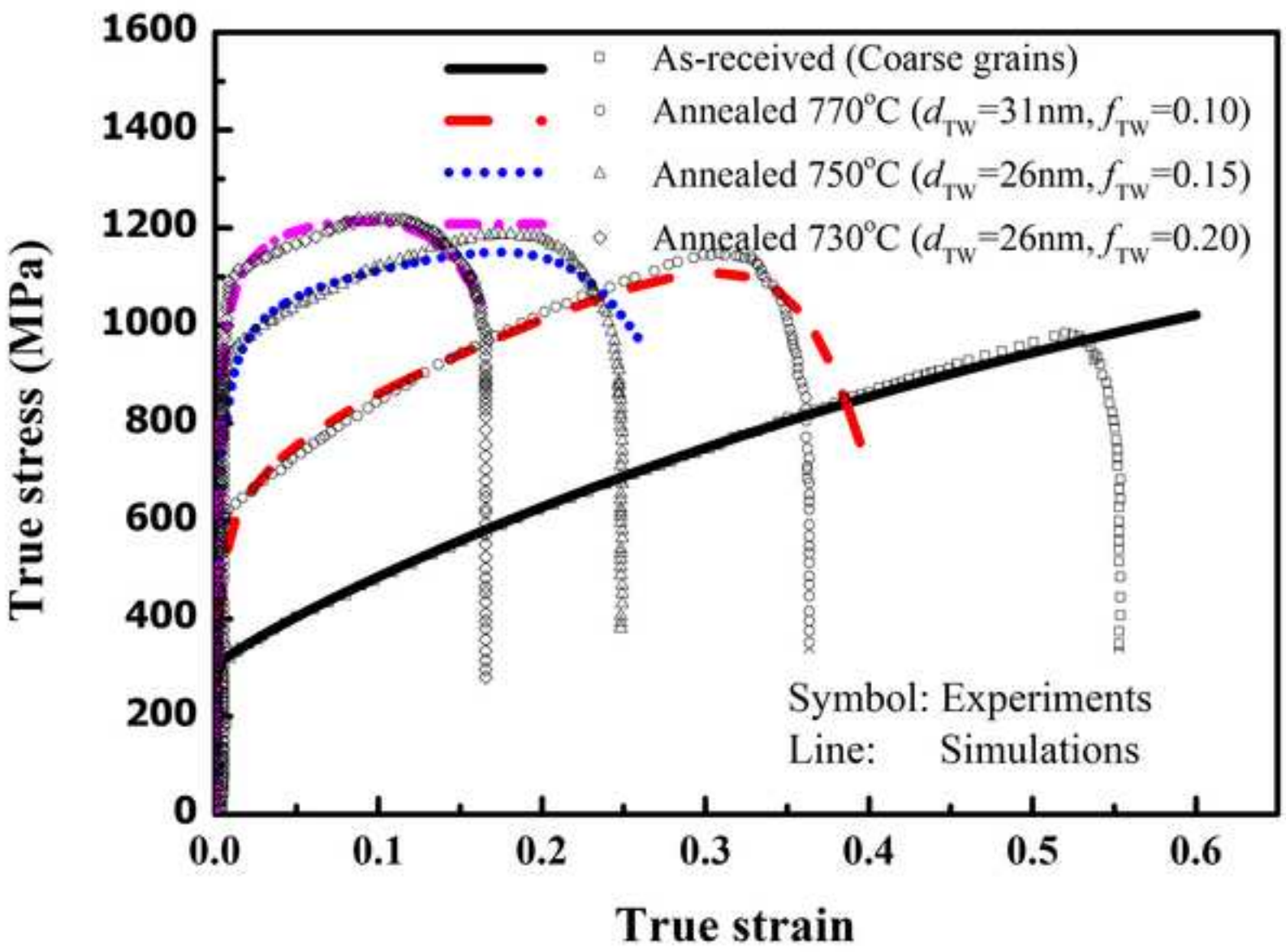

Figure4
Click here to download high resolution image

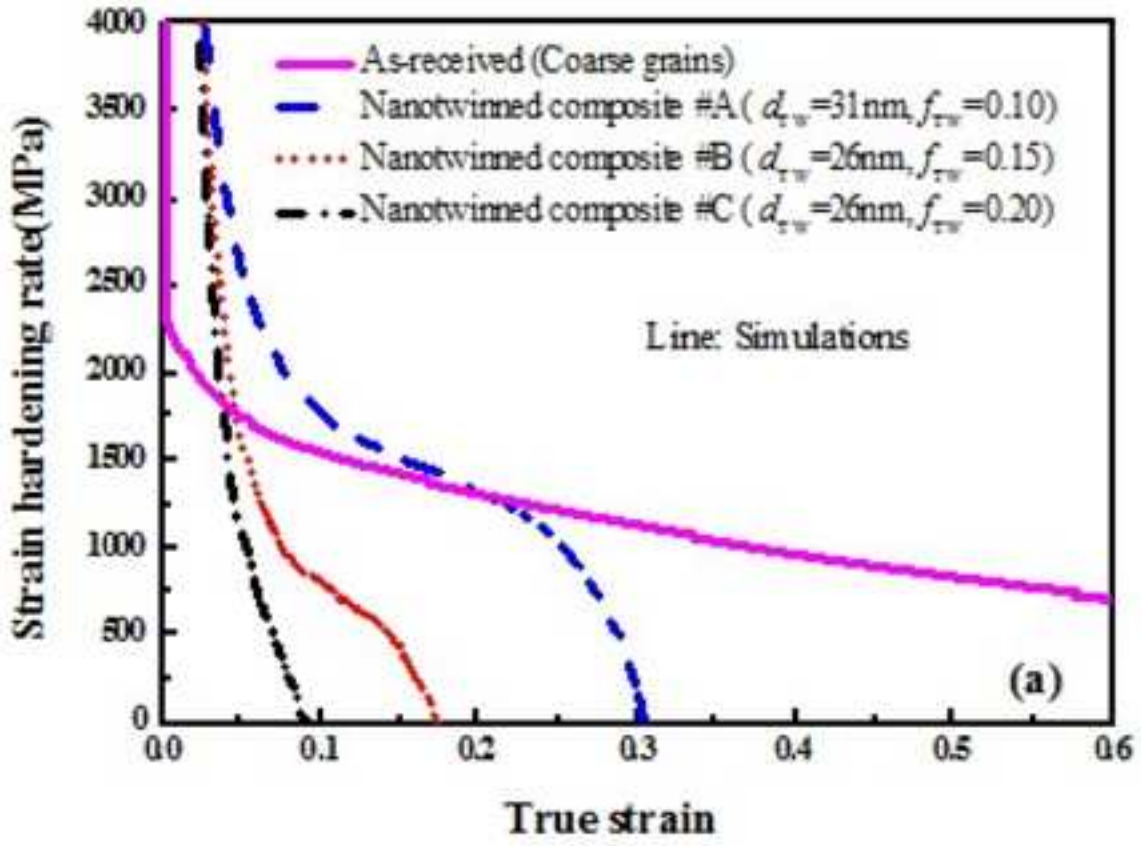

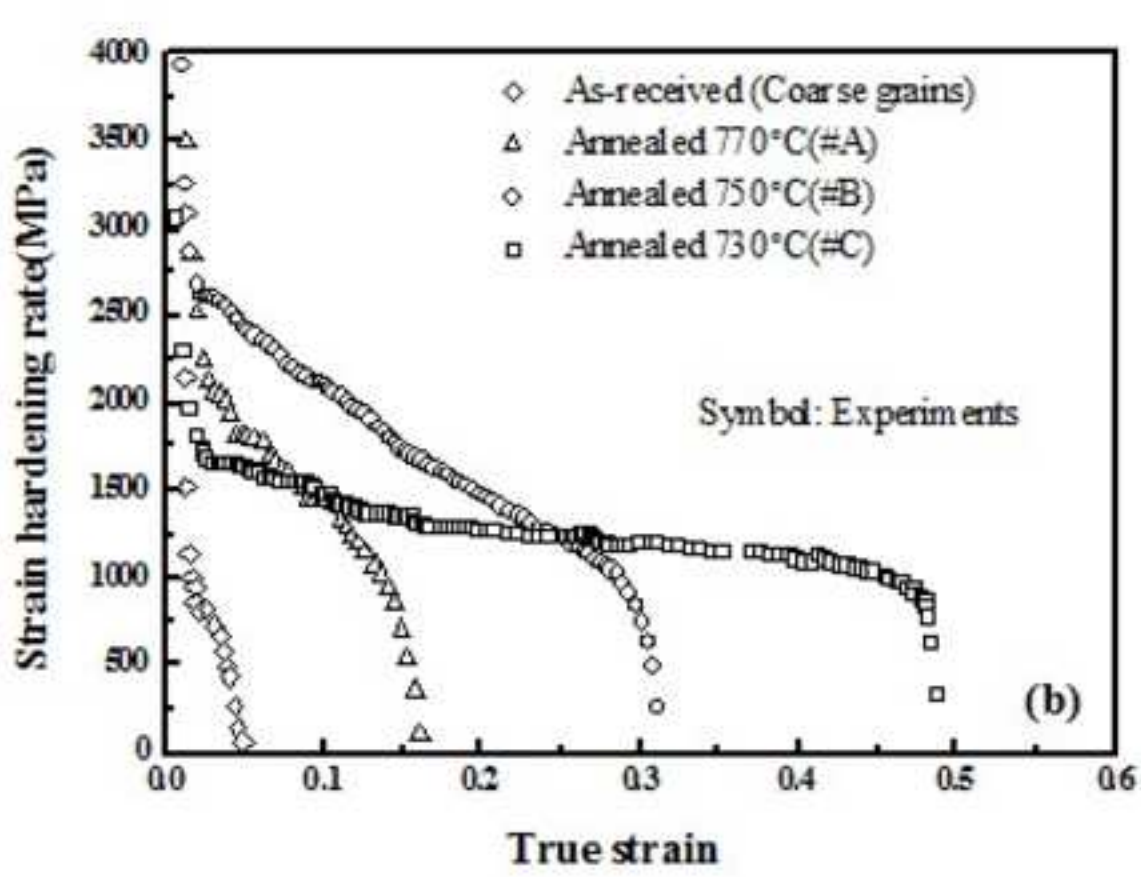

Figure5
Click here to download high resolution image

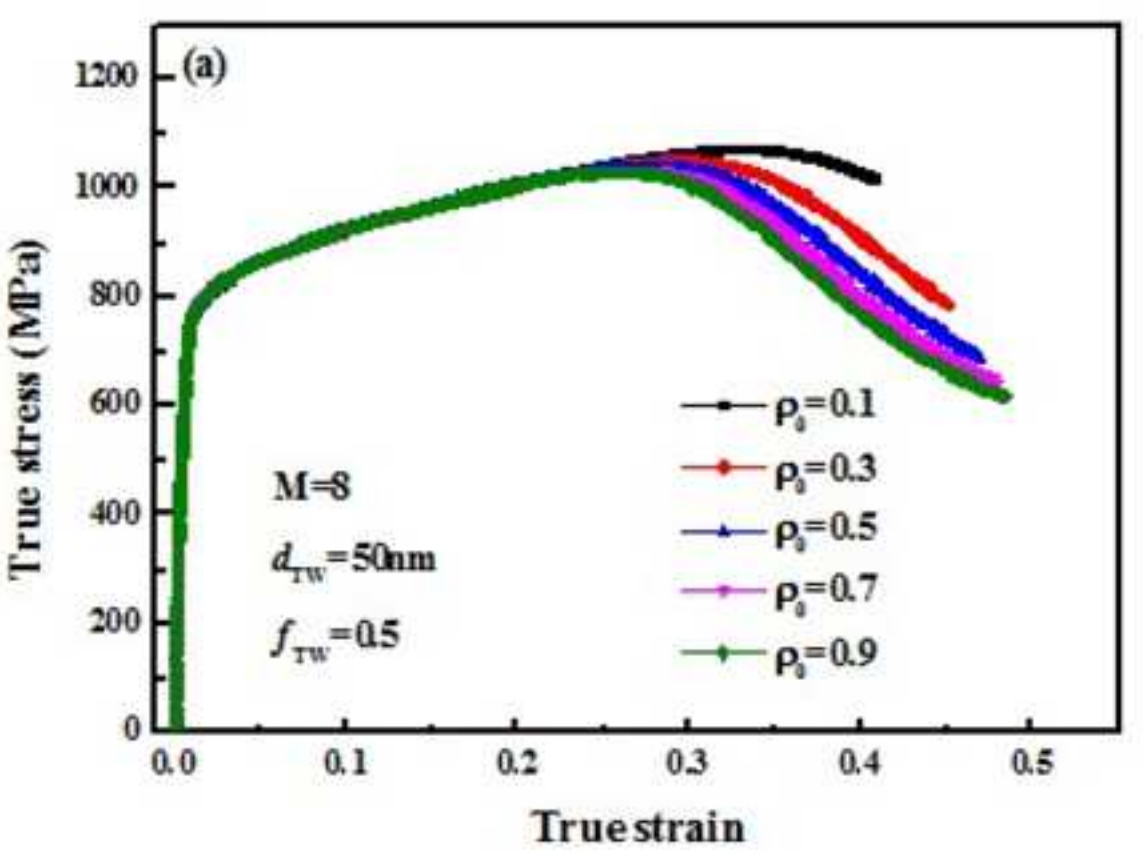

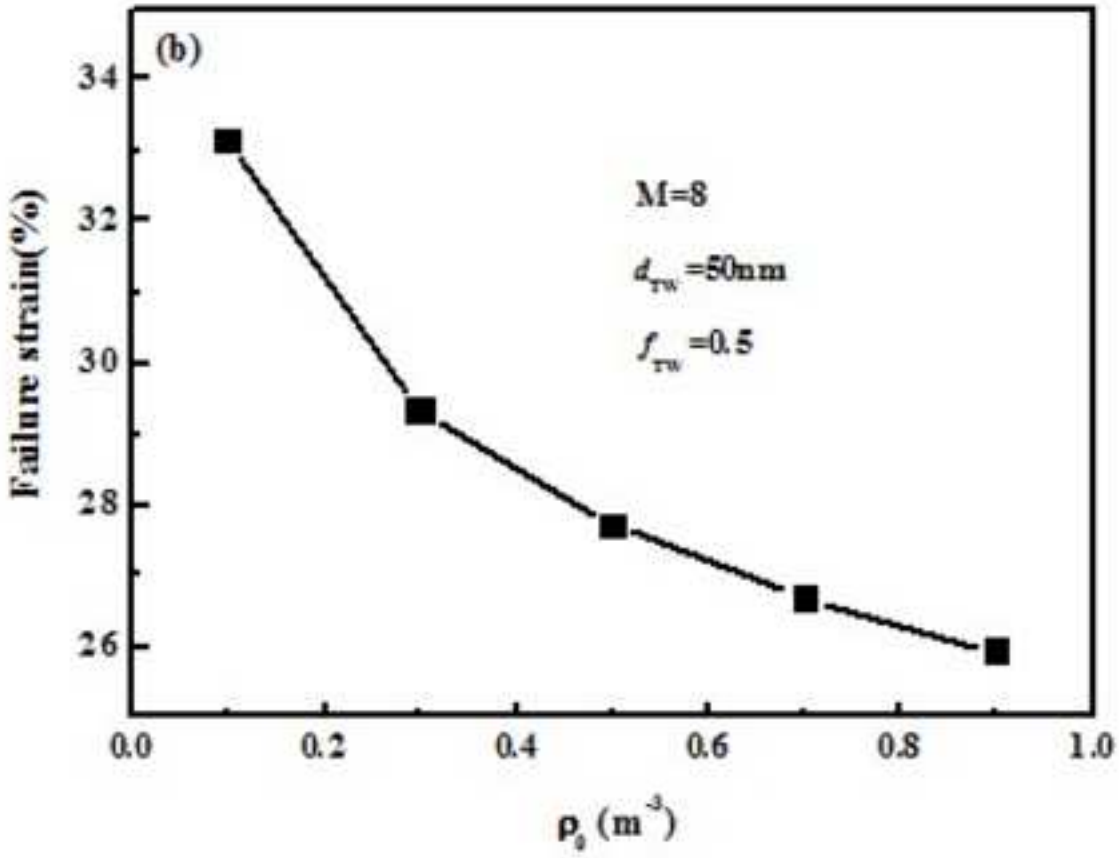

Figure6
Click here to download high resolution image

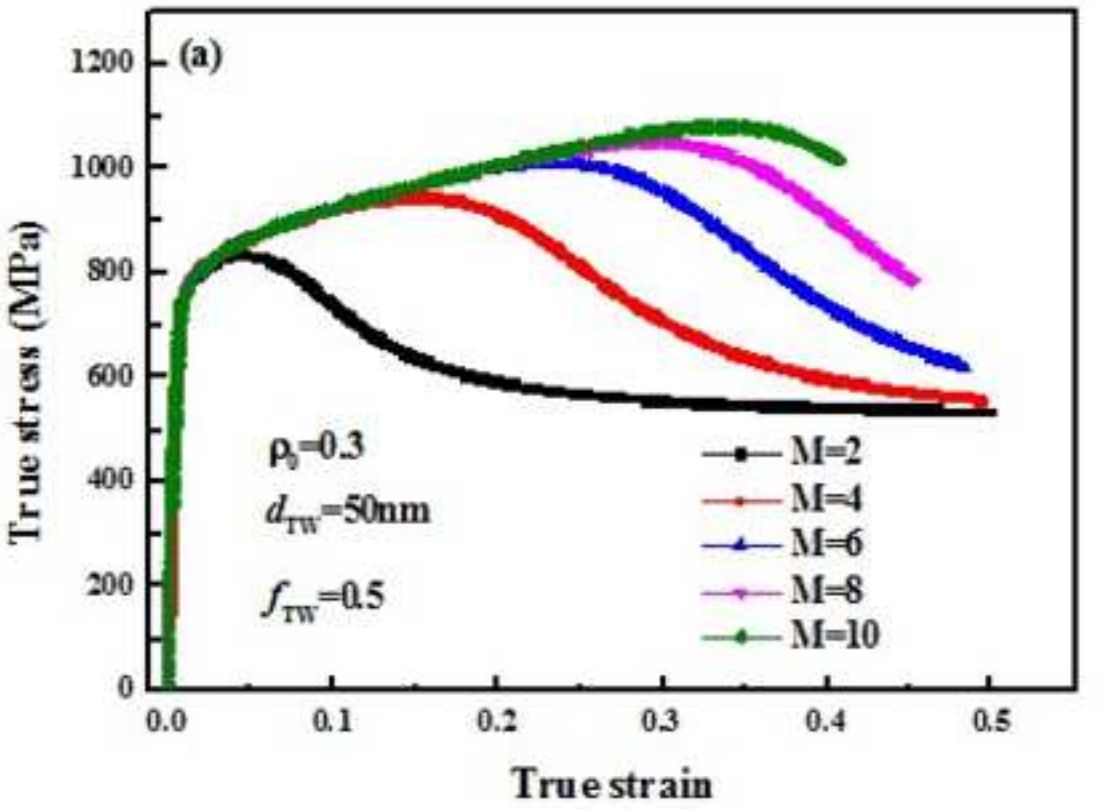

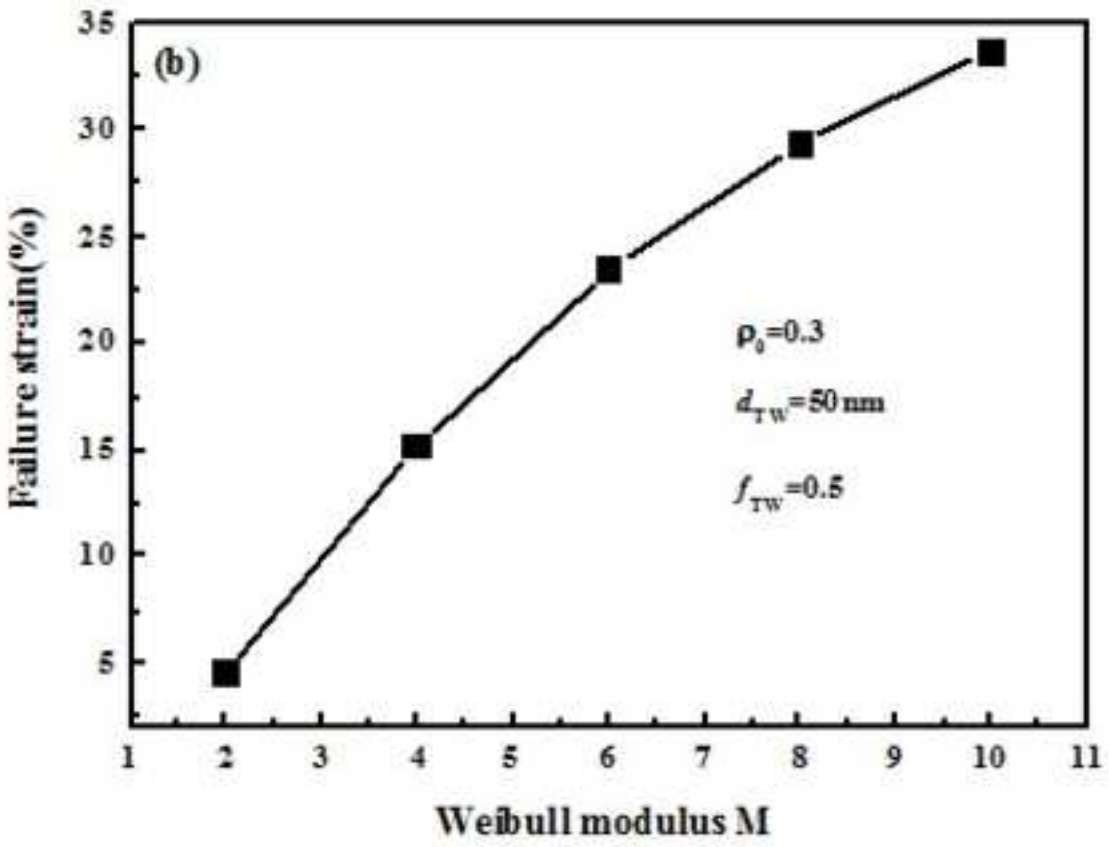

Figure7
Click here to download high resolution image

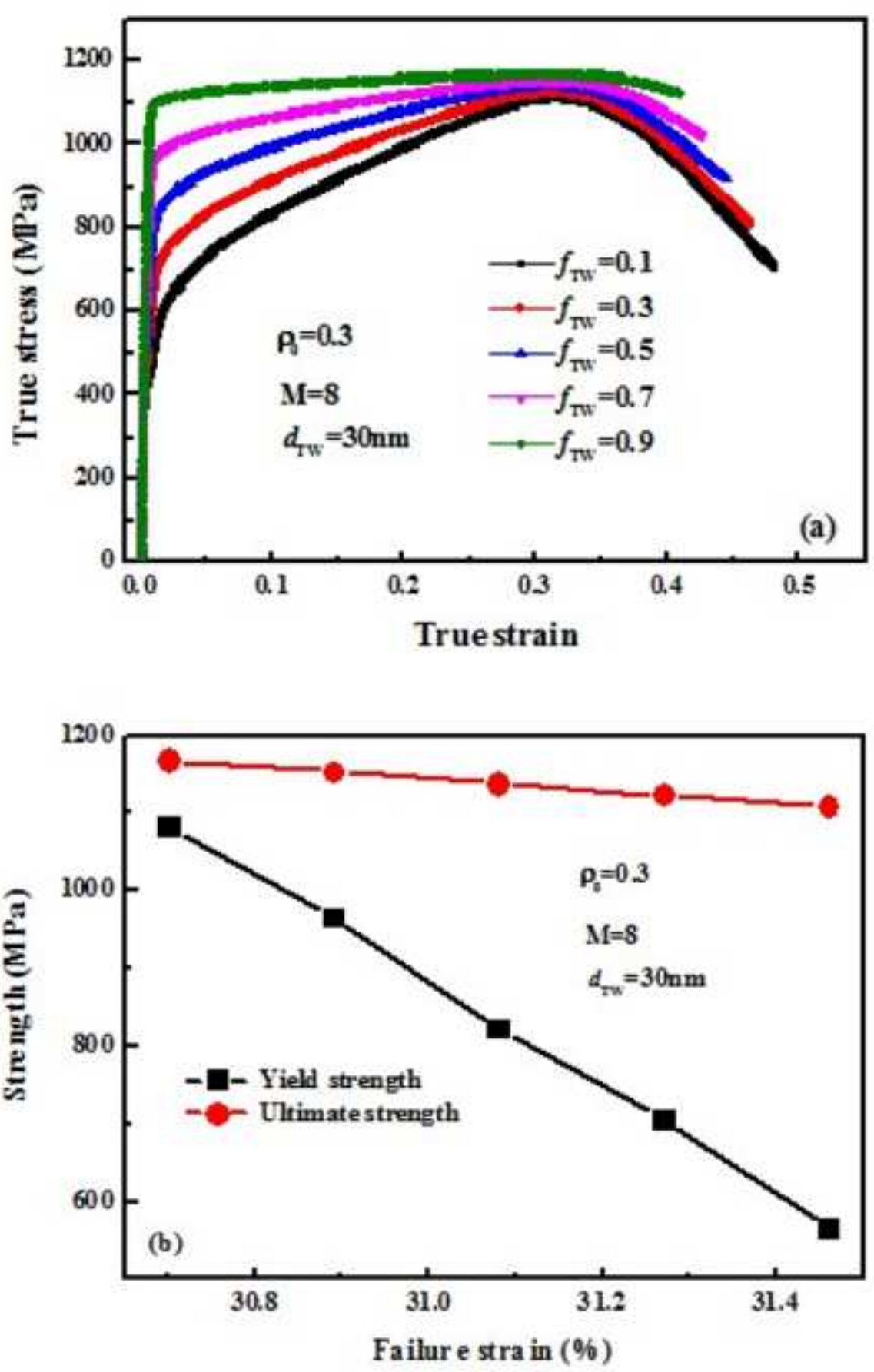

Figure8

Click here to download high resolution image

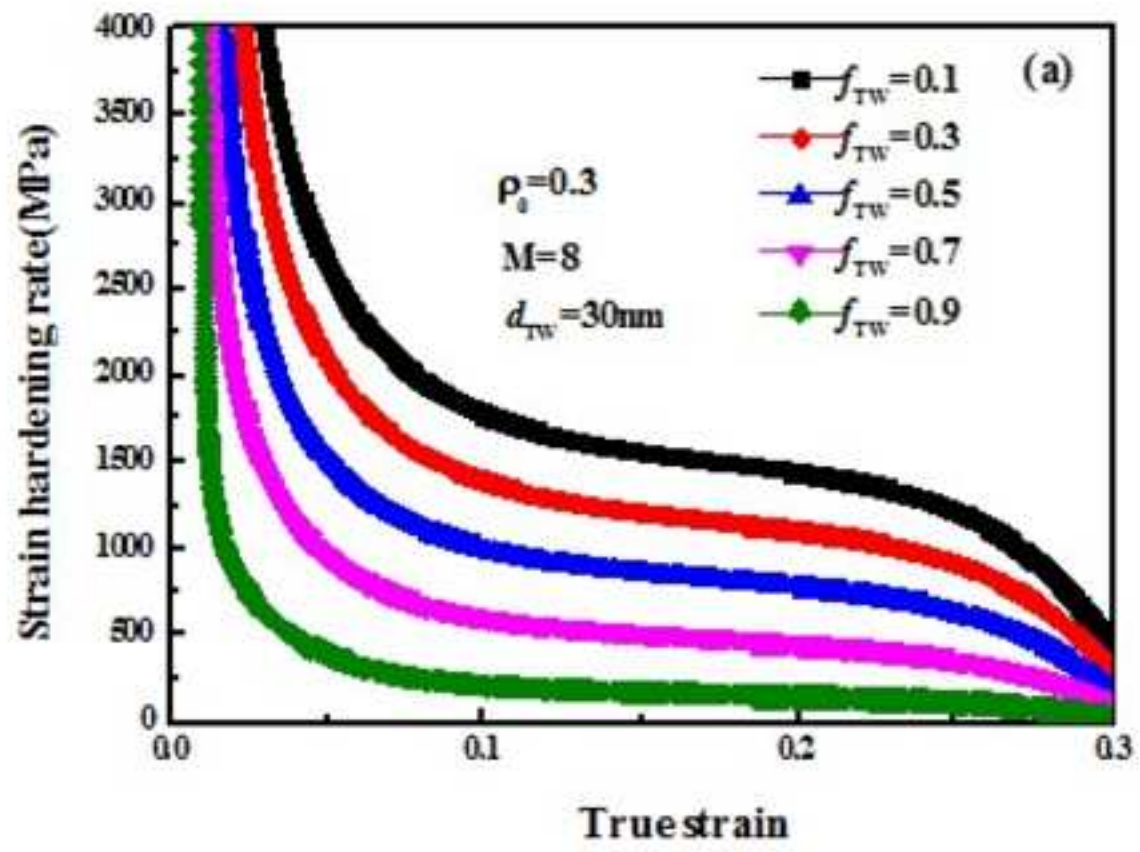

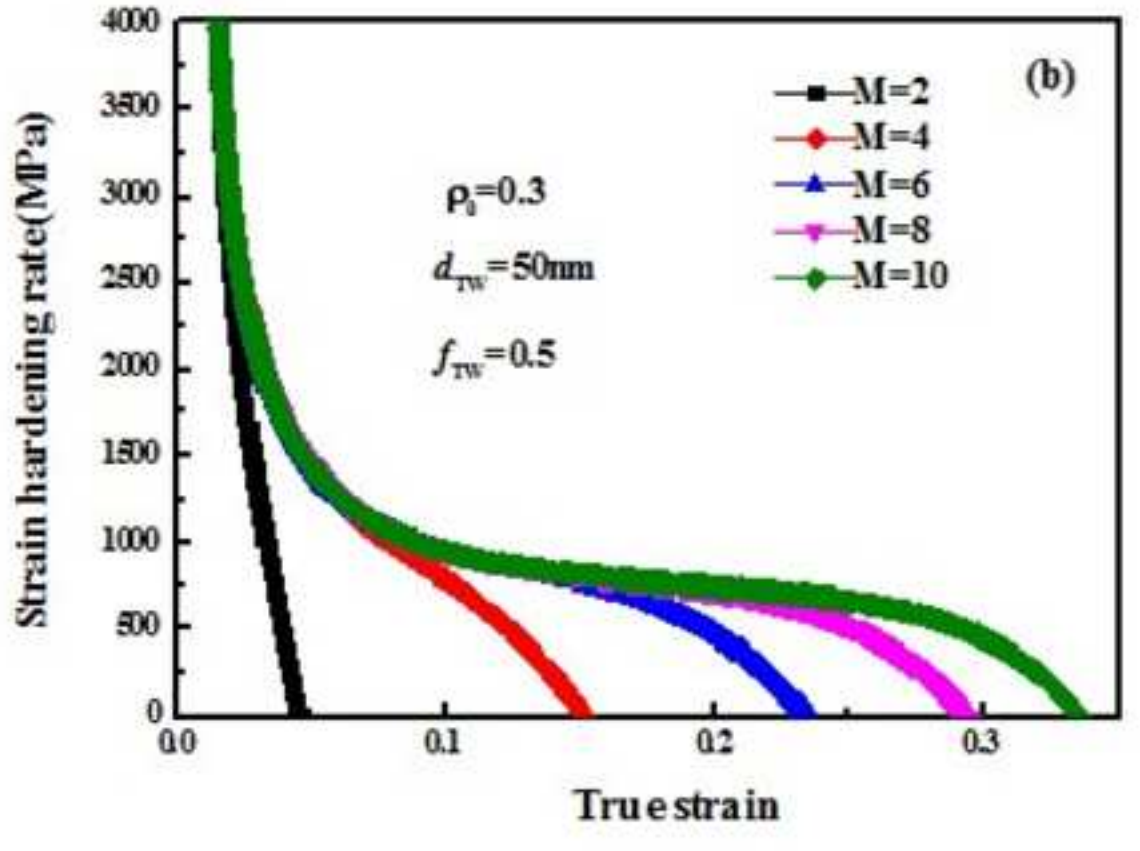

Figure9
Click here to download high resolution image